European Journal of Pharmaceutics and Biopharmaceutics 180 (2022) 149–160

Contents lists available at ScienceDirect

European Journal of Pharmaceutics and Biopharmaceutics

journal homepage: www.elsevier.com/locate/ejpb

Research paper

DoE-based development of celecoxib loaded PLGA nanoparticles: In ovo assessment of its antiangiogenic effect

Mario Alonso-González [a], Ana Fernández-Carballido [a,b], Prissila Quispe-Chauca [a], Irene Lozza [a], Cristina Martín-Sabroso [a,b], Ana Isabel Fraguas-Sánchez [a,b,*]

[a] Department of Pharmaceutics and Food Technology, Faculty of Pharmacy, Complutense University of Madrid, Spain
[b] Institute of Industrial Pharmacy. Faculty of Pharmacy, Complutense University of Madrid, Spain

ARTICLE INFO

Keywords:
Angiogenesis
COX-2 inhibitors
Inflammation
Nanomedicine
Plackett-Burman design
Polymeric nanoparticles
Yolk sac model (YSM)

ABSTRACT

Abnormal angiogenesis plays a main role in the pathogenesis of many diseases such as cancer, and inflammatory autoimmune disorders among others, and its inhibition represents a potential strategy for their management. Celecoxib (CXB) that is one of the most prescribed selective COX-2 inhibitors and is currently approved for the treatment of osteoarthritis, rheumatoid arthritis, and ankylosing spondylitis inhibits angiogenesis. The objective of this manuscript was to design, develop, and characterize polymeric nanoparticles for the parenteral administration of CXB which the aim of facilitating its administration and improving its antiangiogenic activity while decreasing its adverse effects. A Plackett-Burman design was used to optimize the formulation. The PVA concentration, the sonication time, the sonicator amplitude and the CXB:PLGA ratio were selected as independent variables and particle size, polydispersity index, drug loading, and entrapment efficiency as responses. Optimized nanoparticles (formulations F2, F6 and F9) showed a particle size around 280 nm, a low polydispersion (PDI $\leq$ 0.2), a negative zeta potential around −25 mV, a high entrapment efficiency (above 88 %) and a controlled drug release for at least 10 days. Moreover, they were physically and chemically stable for at least 3 months when stored at 4 °C. Interestingly, CXB-loaded nanoparticles showed a higher angiogenesis inhibition than CXB in solution administered at the same concentration. F9 nanoparticles that were prepared using PVA at 0.5 %, a sonication time of 7 min, a sonicator amplitude of 80 % and a CXB:PLGA ratio of 20:100 were selected as the most suitable CXB-formulation. It represents a promising strategy to administer CXB and improve its efficacy in disorders with pathological angiogenesis such as cancer and arthritic diseases.

1. Introduction

Angiogenesis consists of the formation of new capillaries from pre-existing vasculature and is essential for several physiological processes such as organ growth during embryonic development and wound healing. Abnormal angiogenesis also plays a main role in the pathogenesis of many diseases such as cancer, and inflammatory autoimmune disorders among others [1,2]. For example, in tumors, excessive vasculature fosters tumor growth, the migration of tumoral cells, and metastases formation [3]. In rheumatoid arthritis angiogenesis contributes to disease progression as it promotes the accumulation of inflammatory cells into the joints, resulting in synovial hyperplasia and pannus formation, and, consequently, gradual bone destruction [4,5]. In this context, the inhibition of this pathological vascularization can be beneficial. In cancer disease, it contributes to reduce tumor growth and metastases formation. In rheumatoid arthritis the use of antiangiogenic compounds can palliate synovitis and pannus formation, relieving the inflammation, pain, and swelling of these patients [6].

Non-steroidal anti-inflammatory drugs (NSAIDs) represent one of the most widely used medications worldwide due to their analgesic and anti-inflammatory properties [7]. However, their long-term use can produce gastrointestinal damage causing irritation, ulcers, dyspepsia, gastrointestinal bleeding, and diarrhea among other symptomatology. Their anti-inflammatory activity is attributed to the inhibition of prostaglandin synthesis by blocking cyclooxygenase (COX), and two different isoforms of this enzyme have been characterized: COX-1 and COX-2. While COX-1 is expressed in the stomach and its inhibition is related to the gastrointestinal toxicity of NSAIDs, the COX-2 isoform is induced in inflammation situations and observed in the inflammatory cells. As a result, the use of selective COX-2 inhibitors is beneficial as

* Corresponding author at: Department of Pharmaceutics and Food Technology, Complutense University of Madrid, Spain.
E-mail address: aifraguas@ucm.es (A. Isabel Fraguas-Sánchez).

https://doi.org/10.1016/j.ejpb.2022.09.022
Received 22 July 2022; Received in revised form 7 September 2022; Accepted 25 September 2022
Available online 8 October 2022

they show lower gastrointestinal damage [8,9]. Celecoxib (CXB) is one of the most prescribed and used selective COX-2 inhibitors.

CXB is currently approved by FDA and EMA for the treatment of osteoarthritis, rheumatoid arthritis and ankylosing spondylitis [10]. Moreover, it has shown promising potential in the prevention and treatment of several carcinomas, mainly colon, breast, prostate, ovarian, and head and neck cancers. CXB inhibits vascularization [11,12] which is responsible, at least in part, for its anticancer activity and it is beneficial for the treatment of inflammatory disorders.

Despite the therapeutic utility of CXB, it is not devoid of serious adverse effects, being related to thrombotic cardiovascular events and renal adverse effects, especially after chronic treatments like occurs in the pathologies where it is useful [13,14]. Moreover, its high lipophilicity (solubility in water: 4.3 mg/L) limits its oral bioavailability and hampers the development of effective formulations, especially parenterally administered formulations [15].

In this context, CXB nanoencapsulation would be beneficial to resolve its administration challenges and optimize the therapeutic use of this drug by decreasing its adverse effects and improving its efficacy [16,17]. In fact, several authors have demonstrated that nanoparticles represent a good tool to administer CXB [18,19]. Moreover, it should be mentioned that nanoencapsulation has improved the activity of other antiangiogenic compounds [20,21]. This indicates that the administration of nano-encapsulated CXB may increase its antiangiogenic effect.

The objective of this manuscript was to design, develop, and characterize polymeric nanoparticles for the parenteral administration of CXB to improve its antiangiogenic activity and decrease its adverse effects. A DoE approach was used to optimize CXB-loaded nanoparticles and establish the influence of several factors during the elaboration process on particle characteristics. Due to its high biocompatibility and high biodegradability, poly-lactic-*co*-glycolic acid (PLGA) which is approved by FDA and EMA for human use, was selected as polymer [22].

2. Materıal and methods

2.1. Materıals

CXB was obtained from Hangzhou Onion Chemical Co. Ltd. (China). Poly-(lactide-*co*-glycolic acid-resomer RG® 502 (PLGA-502) (i.v. 0.16–0.24 dL/g) was purchased from Evonik® Industries (Essen, Germany). Polyvinyl alcohol (PVA, Mw = 30,000–70,000), was supplied by Sigma-Aldrich (St. Louis, MO, USA). HPLC-grade methanol, ethanol, dichloromethane (DCM) and sodium lauryl sulphate (SLS) were obtained from Fisher Scientific (Frederick, MA, USA). Potassium dihydrogen phosphate (KH2PO4) and disodium hydrogen phosphate dehydrate (Na2HPO4_2 H2O) were provided by Panreac (Barcelona, Spain). Demineralized Milli-Q® water (Millipore, Madrid, Spain) was used to prepare all buffers and solutions. All chemicals and reagents were used as received.

2.2. Formulation and optimization of CXB-loaded nanoparticles

2.2.1. Experimental design

A two-level Plackett-Burman (PB) experimental design was performed for the development of CXB-loaded-PLGA nanoparticles (CXB-PLGA-Nps) to determine the critical factors in the preparation of these nanoparticles that influences on four main nanoparticle characteristics (responses): particle size, polydispersity index (PDI), drug loading (DL) and entrapment efficiency (EE). The factors screened were the following: PVA concentration, sonication time, sonicator amplitude and CXB:PLGA ratio (independent variables). Table 1 displays the used experimental design. This design of experiments, as well as the statistical evaluation of the variables in each of the responses, was carried out using the Minitab® 19 program (Pennsylvania-USA) [23]. In this DOE a total of 12 formulations (F1-F12) were prepared.

Table 1
Plackett-Burman experimental design.

	Experimental value	
Independent Variables	**Low (-1)**	**High (+1)**
PVA concentration (%)	0.5	3
Sonication time (minutes)	2	7
Amplitude of the sonicator (%)	50	80
Ratio CXB:PLGA (m/m)	5:100	20:100

2.2.2. Elaboration of CXB-loaded nanoparticles

CXB-PLGA-Nps were prepared using PLGA-RG®-502 as polymer by the solvent emulsification-evaporation method. Dichloromethane was used as organic solvent and PVA solution (0.5 and 3 %) as aqueous external phase. Briefly, 100 mg of PLGA 502 and 5 mg or 20 mg of CXB were dissolved in 1 ml of dichloromethane. This solution was added dropwise over the aqueous phase under stirring. Then, it was sonicated (Fisher Scientific sonicator, Fisher Scientific, Frederick, MA, USA) for 2 or 7 min at a sonication amplitude of 50 or 80 %. A 40/20 s on/off pulse was used. To allow solvent evaporation, the resulting nanoparticle suspension was stirred for 3 h at 500 rpm at room temperature. After this, nanoparticles were collected by centrifugation at 13000 rpm for 40 min. This process was repeated twice more, resuspending the nanoparticles in MiliQ-water, to wash the nanoparticles and remove the PVA residues. After the last centrifugation, the supernatant was removed, the nanoparticles were suspended in 1 ml of 3 % sucrose solution (added as cryoprotectant) and stored at −20 °C for 24 h. Finally, they were lyophilized for 36 h at 50 °C and 0.2 mbar (Telstar Lyoquest® Tokyo, Japan).

2.3. Characterization of CXB-loaded nanoparticles

2.3.1. Particle size, PDI, and zeta potential

The mean particle size (expressed as volume diameter) and PDI of developed nanoparticles were determined by dynamic light scattering using a Microtrac®-Zetatrac Particle Analyzer (Microtrac Inc., Montgomeryville, PA, USA). Zeta potential was evaluated by a laser-Doppler anemometry using a Malvern Zetasizer (Malvern Instruments, Worcestershire, UK) [24].

2.3.2. Drug loading, entrapment efficiency and process yield

Drug loading and entrapment efficiency of CXB-PLGA-Nps was determined by HPLC following the protocol described by Vera et al. [25]. A C18 Mediterranea Sea HPLC column (25 cm, 5 μm particle size) (Tecnokroma, Spain) was used. A mixture of water:methanol (25:75) was used as mobile phase at a flow rate of 1 ml/min. Briefly, 7.5 mg of freeze-dried nanoparticles were weighted and dissolved in 0.5 ml of DCM. Then 12 ml of ethanol was added with the aim of extracting CXB and precipitating PLGA. Finally, the samples were filtered and analyzed by HPLC. EE was calculated using the following equation:

$$EE(\%) = \frac{CXB : PLGAratioexperimental}{CXB : PLGAratioinitial} x100 \quad (1)$$

Process yield of freeze-dried nanoparticles was calculated as follows:

$$Process\ yield(\%) = \frac{Wtotal}{WPLGA + WCXB + Wsucrose} \quad (2)$$

where W_{total} is the total weight of nanoparticles, W_{PLGA} and W_{CXB} are the weight of polymer and drug used in each formulation respectively and $W_{sucrose}$ is the amount of sucrose added as cryoprotectant.

2.3.3. Morphological examination

The shape and surface morphology of selected NPs (F2, F6, F9) were analyzed by scanning electron microscopy (SEM; JEM 6335F; JEOL, Tokyo, Japan) as described in [26]. Firstly, cryoprotectant was eliminated by suspending nanoparticles in MiliQ-water and centrifuging the

resulting suspension at 13000 rpm for 20 min. This step was repeated thrice. Then, a drop of nanoparticle suspension (100μg/ml) was added to a coverslip adhered to a stub and maintained in a desiccator for 24 h. Then, dried samples were coated with a gold–palladium mixture and examined by SEM.

2.3.4. Drug release studies

In vitro release study of CXB from selected CXB-PLGA-Nps (F2, F6, F9) was carried out in a heated bath (WB22; Memmert GmbH, Schwabach, Germany) at 37 °C ± 0.2 °C and constant shaking of 100 rpm as previously described with some modifications [27]. 20 mg of nanoparticles were suspended in 10 ml phosphate-buffered saline (PBS) at pH 7.4 containing LSS at 1 % to maintain sink conditions. At regular time intervals, samples were centrifuged, 1 ml of the supernatant was removed, filtered through 0.22 nm filters, and measured by HPLC. 1 ml of fresh PBS was added to maintain a total volume of 10 ml during the study.

2.3.5. Stability studies

The physical and chemical stability of CXB-PLGA-Nps during storage for 3 months was evaluated. Briefly, freeze-dried nanoparticles were stored at 5 ± 3 °C. At predetermined time points (1, 2 and 3 months), nanoparticles were suspended in MiliQ-water. Then, particle size, polydispersity index, and CXB content were determined.

2.4. Angiogenesis studies

The anti-angiogenic effect of CXB-PLGA-Nps was evaluated in the chick embryo model, one of the most established models for the study of angiogenesis [28,29] using the yolk sac membrane (YSM) assay as previously described with some modifications [30]. Pathogen-free fertilized chicken eggs were incubated at 38 °C and 47 % of humidity in an automated egg incubator under rotation. At embryo development day (EED) 2.5, egg viability was checked. In viable eggs, a drill aperture in the narrow part of the egg was done and 2–3 ml of albumen were removed. The aperture was sealed, and the eggs were placed in the incubator. Then, at EDD 3 the window was slightly enlarged. After, 1 h of accommodation, 200 μL of CXB in solution at 100 μM or the equivalent amount of CXB-PLGA-Nps suspended in NaCl 0.9 % (the amount of nanoparticles was calculated using release study data) were added. The blood vessels were photographed after 48 h. The number of blood vessels (primary, secondary, tertiary and quaternary) was quantified using Image-J software. Eggs treated with NaCl 0.9 %, and arginine (50 μ/mL) were used as negative and positive control of angiogenesis respectively. At least 5 eggs were used/treatment.

2.5. Data analysis

PBD was designed and analyzed using Minitab 19 software (Minitab Inc., State College, Pennsylvania, USA). The data was reported as a mean ± S.D (standard deviation) of at least three experiments (n = 3). While multiple groups were compared using one-way variance analysis (ANOVA), the statistical differences between two groups were determined using a *t*-Student test using Statgraphics 19 software (Statgraphics Technologies, Inc., Virginia, USA). Significant differences were reported as follows: *0.01 < p < 0.05 and **p < 0.01. All the graphs were compiled using Origin 2019 software (Origin lab, Massachusetts, USA).

3. Results and discussion

3.1. Plackett-Burman design

A Plackett-Burman design, widely used for the development and optimization of nanoformulations [31–33], has been carried out to determine the influence of several independent variables: PVA concentration, sonication time, the amplitude of the sonicator and polymer:drug ratio on main characteristics (particle size, PDI, drug loading and entrapment efficiency) of CBX-loaded nanoparticles. A total of 12 formulations were prepared whose characteristics are described in Table 2.

3.1.1. Influence on particle size

As displayed in Table 2, all CXB-PLGA-Nps showed an average size, expressed as volume diameter, between 207 and 365 nm. The statistical analysis of the effect of independent variables on the particle size of CXB-PLGA-Nps is described in Table 3. The value of the correlation coefficient was found to be close to 0.9 ($R^2 = 0.8808$), indicating that>88 % of the variation in the response (particle size in this case) can be explained by the model. This is also confirmed by the p-value obtained from the model (p-value < 0.01). The model had no lack of fit, as the p-value of this test (0.929) was higher than 0.05. The equation of the regression model for particle size is given below:

$$SIZE(nm) = 458.9 - 26.95A - 10.69B - 1.306C + 0.715D \quad (3)$$

where A represents the PVA concentration (%), B the sonication time (min), C the sonicator amplitude (%) and "D" the ratio of PLGA: CXB used. The different coefficients obtained in this equation represent the quantitative effect of all these independent variables on the particle size. The sign of the coefficient indicates the relationship between the two variables, so a negative sign indicates that the higher the value of the independent variable, the lower the value of the response [33].

As displayed in the Pareto diagram corresponding to particle size (Fig. 1A), PVA concentration, sonication time and sonicator amplitude had a statistically significant effect (p-value < 0.05) on particle size (Table 3). In all cases, these three variables have a negative effect on this response, so that an increase in any of these variables implies a decrease in particle size, as indicated by the negative signs obtained in the equation (Eq.3). PVA concentration, followed by sonication time, are the variables that had the greatest influence. These results are similar to those obtained by other authors in the elaboration of PLGA nanoparticles by the solvent emulsification-evaporation method. In most of the formulations, an increase in the surfactant concentration, PVA in this case, implies a decrease in the particle size [34,35] due to a greater stabilization of the emulsion. However, some authors have found that an increase in PVA concentration results in larger particle size [36], which may be attributed to the slower evaporation of the solvent due to the increase in viscosity of the aqueous phase of the emulsion that occurs when PVA concentration is increased. Probably the PVA concentrations (1–3 %) used in this work, have not implied such a high increase in viscosity that slows down the evaporation of the DCM and leads to larger nanoparticles. In general, an increase in sonicator amplitude and sonication time also triggers a decrease in particle size due to the increase in energy applied during the emulsification process, which allows the formation of smaller droplets and thus smaller nanoparticles [36,37]. Finally, unlike the other three variables studied, the PLGA:CXB ratio does not have a statistically significant influence on particle size (Fig. 1A), with a p-value > 0.05 (Table 5). Fig. 2 shows the contour plot of particle size vs PVA concentration, sonication time, sonicator amplitude, and CXB:PLGA ratio.

Particle size is a critical factor for the administration of nanoparticles. The developed nanoparticles are intended to be administered by a parenteral route. In this case, all obtained formulations show a suitable particle size to be administered intravenously [38]. Moreover, their particle size is also suitable for intracavitary administration routes (e.g intraarticular, intraperitoneal) as these formulations would allow the localization of the drug at the action site. For example, Thakkar and coworkers demonstrated that lipid nanoparticles of around 250 nm were efficiently retained in inflamed joints when administered by this route [39]. In this work, except F3, F10, F11 and F12 formulations that have a mean particle size below 250 nm, we hypothesized that the developed nanoparticles could be retained in the intraarticular cavity. These

Table 2
Experimental design and characteristics of CXB-PLGA-Nps.

Formulation	PVA (%)	Sonication time (min)	Amplitude (%)	CXB: PLGA ratio	Particle size ± sd (nm)	PDI ± sd	Drug loading (mg CXB/10 mg Nps) ± sd	EE (%) ± sd
F1	0.5	2	50	20:100	362.01 ± 9.64	0.26 ± 0.06	1.19 ± 0.22	71.53 ± 9.24
F2	0.5	7	80	5:100	273.03 ± 19.09	0.20 ± 0.01	0.44 ± 0.48	93.21 ± 20.15
F3	3	7	80	5:100	207.30 ± 5.45	0.08 ± 0.03	0.30 ± 0.47	63.73 ± 4.16
F4	0.5	2	50	5:100	359.33 ± 11.59	0.32 ± 0.04	0.45 ± 0.76	93.86 ± 1.73
F5	3	2	50	5:100	304.63 ± 10.03	0.13 ± 0.01	0.44 ± 0.74	92.62 ± 2.54
F6	3	7	50	20:100	284.66 ± 7.98	0.14 ± 0.04	1.47 ± 0.46	88.63 ± 19.52
F7	0.5	2	80	20:100	320.60 ± 4.60	0.22 ± 0.01	1.40 ± 0.20	84.39 ± 8.50
F8	0.5	7	50	5:100	275.55 ± 14.29	0.29 ± 0.12	0.40 ± 0.62	83.12 ± 5.02
F9	0.5	7	80	20:100	287.80 ± 10.85	0.09 ± 0.02	1.56 ± 0.12	93.85 ± 5.11
F10	3	7	50	20:100	217.50 ± 12.50	0.09 ± 0.09	1.24 ± 0.34	74.53 ± 14.64
F11	3	2	80	20:100	245.77 ± 2.95	0.09 ± 0.01	1.52 ± 0.05	91.58 ± 2.10
F12	3	2	80	5:100	234.20 ± 9.99	0.12 ± 0.06	0.32 ± 0.53	67.67 ± 2.24

Table 3
Statistical ANOVA analysis results of particle size. * Statistically significant differences (p-value ⟨005).

	F-Value	P-value
Regression model	12.93	0.002*
Independent Variables		
• PVA concentration (%)	25.94	0.001*
• Sonication time (min)	16.33	0.005*
• Amplitude of the sonicator (%)	8.77	0.021*
• CXB:PLGA ratio	0.66	0.444
ANOVA Lack of fit test		
Lack of fit	0.21	0.929

nanoparticles could be also retained within the peritoneum and, due to the anticancer effect of CXB, could be also useful for the treatment of intraperitoneal carcinomas such as ovarian tumors [26].

3.1.2. Influence on PDI

The lower the PDI value, the lower polydispersion on particle size. In general, it is considered that values of PDI $\leq$ 0.1 indicate that nanoparticles have a monodisperse distribution. PDI values above 0.1 and below 0.3 indicate low-moderate and acceptable polydispersity [40]. As displayed in Table 2, except F4 which showed a PDI value of 0.32, CXB-PLGA-Nps had PDI values lower than 0.3, and even in some cases (F3, F9-F11) lower than 0.1.

Table 4 shows the statistical analysis of the effect of independent variables on the PDI of CXB-PLGA nanoparticles. The obtained coefficient of determination shows a value close to 0.9 ($R^2 = 0.8704$), indicating that around 87 % of the variation in PDI can be explained by the model. This is also confirmed by the p-value obtained from the model (p-value < 0.05). The equation of the regression model for the PDI of the nanoparticles is given below:

$$PDI = 0.4818 - 0.04867A - 0.00833B - 0.002389C - 0.00278D \quad (4)$$

where A represents the PVA concentration (%), B the sonication time (min), C the sonicator amplitude (%) and D the ratio of PLGA:CXB used.

As occurred in particle size analysis, the concentration of PVA and the amplitude of the sonicator had a statistically significant influence (p-value < 0.05) on the PDI, (Fig. 1). PVA concentration was the most influential factor. However, the magnitude of this coefficient was much smaller compared to those obtained in the analysis of the effect on particle size. It showed a negative effect (Eq.4), as the higher the PVA concentration the lower PDI was. An increase in surfactant concentration produces greater emulsion stability and, therefore, less polydispersion [41]. Sonication time and PLGA: CXB ratio had no statistically significant influence on PDI (p-value > 0.05).

Fig. 3 displays contour plots of PDI value vs PVA concentration, sonication time, sonicator amplitude and CXB:PLGA ratio.

3.1.3. Influence on drug loading and entrapment efficiency

As displayed in Fig. 1, CXB:PLGA ratio was the only parameter that showed a statistically significant influence (p value < 0.05) on drug loading. The higher the ratio, the higher the loading. However, none of the factors studied (PVA concentration, sonication time, sonicator amplitude and CXB:PLGA ratio) had a statistically significant influence on the encapsulation efficiency.

As can be appreciated in Table 2, all the formulations developed showed high encapsulation efficiencies, above 60 % in all cases, and even above 90 % in some formulations, indicating the high affinity of celecoxib for PLGA. Indeed, other authors have also obtained high encapsulation efficiencies for celecoxib-loaded PLGA nanoparticles elaborated by the solvent emulsification-evaporation method [42]. However, formulations prepared by nanoprecipitation method using a CXB:PLGA ratio of 10:100 (a ratio within the range evaluated in this work), had encapsulation efficiencies below 50 % [43]. Similar EE values were also found by Pontes-Quero et. al. which developed CXB-loaded nanoparticles made with another polymer (poly-(MVE-*co*-VP-*co*-VC) by nanoprecipitation [16]. These lower EE values can be attributed to the solvent used in this method, acetone, or ethanol, which show a higher and faster diffusion through the external aqueous phase than DCM. This results in greater diffusion of celecoxib to this external aqueous phase and therefore less encapsulation of celecoxib inside the nanoparticles.

Table 5 shows the statistical parameters obtained in the analysis of variance carried out using the Minitab® 19 statistical program to evaluate the effect of the different independent variables studied (PVA concentration, sonication time, sonicator amplitude and CXB:PLGA ratio) on drug loading and encapsulation efficiency. The coefficient of

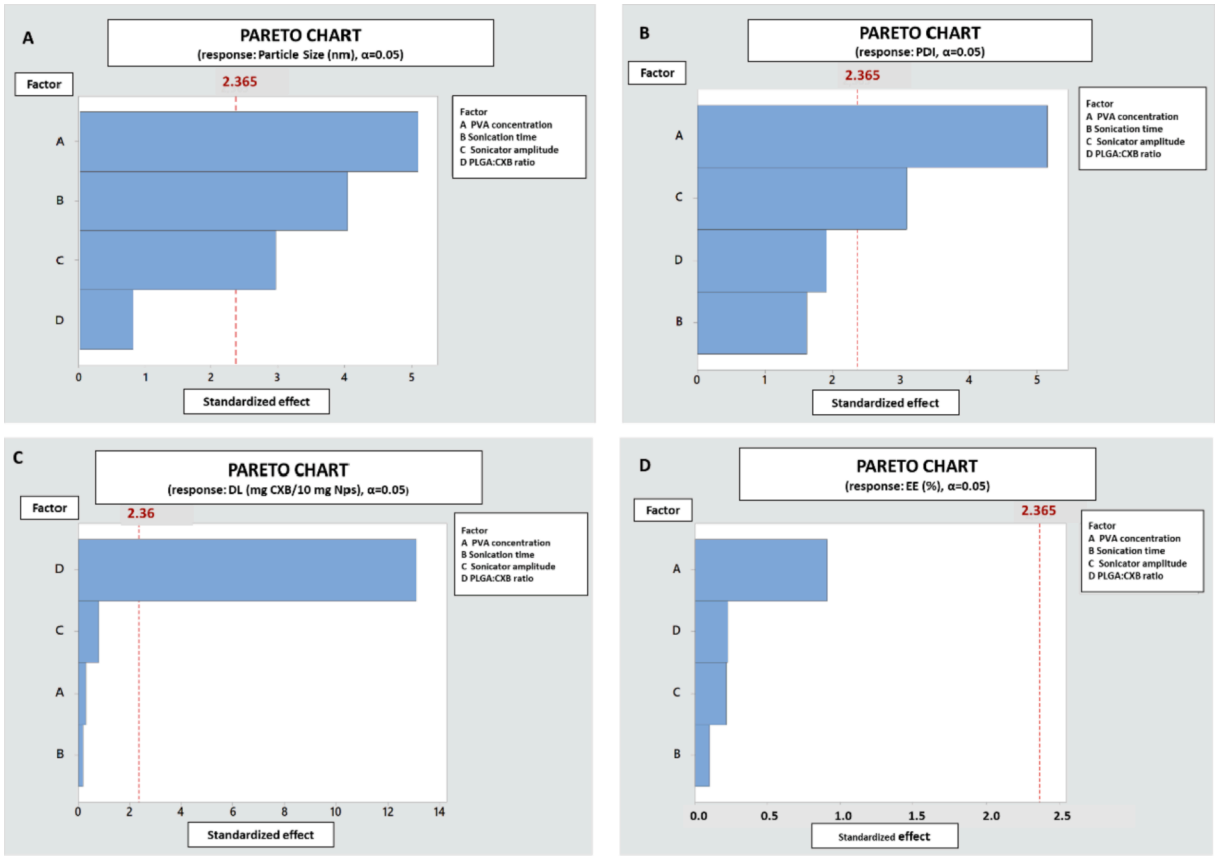

Fig. 1. Pareto chart showing the effect of studied independent variables (PVA concentration, sonication time, sonicator amplitude and CXB:PLGA ratio) on particle size (A), PDI (B), Drug loading (C), and entrapment efficiency (D).

determination obtained for drug loading was close to 1 ($R^2 = 0.961$). However, the coefficient of determination obtained for entrapment efficiency was a very low value ($R^2 = 0.1188$), indicating that only about 11 % of the variation in this response can be explained by the model. This is also confirmed by the p-value obtained from the model (p-value > 0.05). The equations of the regression model for drug loading (Eq. (5)) and entrapment efficiency (Eq. (6)) are as follows:

$$DL\ (mg\ CXB/10\ mg\ Nps) = -0.073 - 0.0092A + 0.0030B + 0.00205C + 0.06692D \quad (5)$$

$$EE(\%) = 90.8 - 2.75A - 0.15B - 0.055C + 0.115D \quad (6)$$

where A represents the PVA concentration (%), B the sonication time (min), C the sonicator amplitude (%) and D the ratio of PLGA:CXB used.

Figs. 4 and 5 display contour plots of PDI value vs PVA concentration, sonication time, sonicator amplitude and CXB:PLGA ratio on drug loading and entrapment efficiency.

Drug loading and entrapment efficiency are important parameters in the development of multiparticulate drug delivery systems. The higher drug loaded into nanoparticles the lower amount of formulation must be administered to reach therapeutic doses. F1, F6, F9 and F11 nanoparticles showed the highest drug loading values (>1 mg of CXB in 10 mg of nanoparticles). All of these formulations were developed with the highest CXB:PLGA ratio (20:100). Entrapment efficiency is an important parameter from a technological point of view, providing information about the limit of the drug:polymer ratio that could be used. Crivelli and co-workers developed CXB nanoparticles using silk fibroin as carrier and found significantly lower EE than the appreciated in this work. These authors found EE values in the interval of 5–11 % in formulations developed with a CXB:polymer ratio 5.25:100 and 12.35:100 [44]. All of this indicates that CXB shows a high affinity for PLGA and that this is a good polymer for its nanoencapsulation. In fact, other authors also developed PLGA nanoparticles loaded with CXB and showed high EE values. However, from a biological point of view drug loading is a more relevant factor as the higher the drug loading the lower amount of nanoparticles must be administered to get a therapeutic effect. Despite the high EE values of the PLGA nanoparticles developed by other authors, their drug loading is significantly lower (maximum 1.05 mg CXB/10 mg Nps) compared with the formulations obtained in this work [42,43].

3.1.4. Plackett Burman design: model validation

Three replications of center checkpoint formulations were elaborated and evaluated for particle size, PDI and drug loading. None of the evaluated factors showed a statistically significant influence on EE (%), probably attributed to the high affinity for PLGA and the fact that formulations were prepared by solvent evaporation technique using DCM as organic phase, which limits CXB diffusion to the aqueous phase during particle formation. Therefore, this response was not validated. Table 6 shows the predicted and observed values of these formulations. The bias percentage was also calculated [45]. The minor differences detected between the average of experimental (observed) values and the predicted ones indicate the validity of the PBD model in providing an adequate prediction of these tested responses: particle size, PDI and CXB loading.

3.2. Characterization of selected formulations

All developed formulations, that showed a particle size in the range of 207–362 nm can be administered intravenously. Moreover, a particle size above 250 nm is desirable to increase the retention time of the

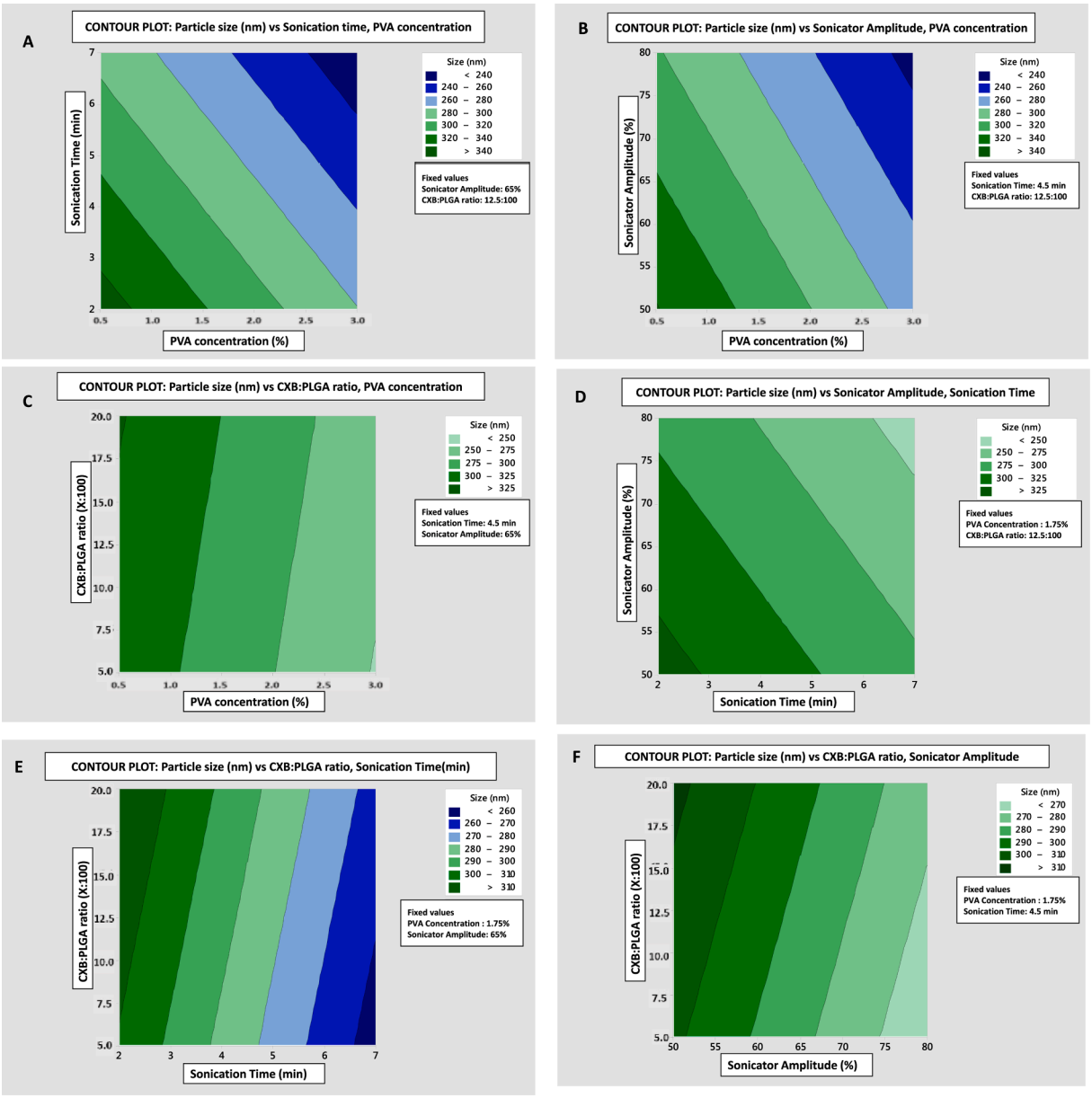

Fig. 2. Contour plots showing the effect of PVA concentration, sonication time, sonicator amplitude, and CXB: PLGA ratio on particle size (nm).

Table 4
Statistical ANOVA analysis results of PDI. * Statistically significant differences (p-value ⟨005).

	F-Value	P-value
Regression model	11.75	0.003*
Independent Variables		
• PVA concentration (%)	29.72	0.001*
• Sonication time (min)	3.49	0.104
• Amplitude of the sonicator (%)	10.31	0.015*
• CXB:PLGA ratio	3.49	0.104
ANOVA Lack of fit test		
Lack of fit	1.23	0.598

nanoparticles when administered intracavitarily. In this context, nanoparticles with a lower particle size below 250 nm were discarded. A low PDI value and a high CXB loading are also desired. F6 and F9 formulations that showed a particle size around 290 nm, low PDI (below 0.15), a high drug loading (≈1.5 mg CXB/10 mg Nps) and EE (%) values of around 90 % were selected for the following experiments. Both formulations were prepared with a CXB:PLGA ratio of 20:100. It has been demonstrated that the higher loading the faster drug release, especially during the first time points [26]. A formulation elaborated with the lowest CXB:PLGA ratio was also selected despite its lower drug loading compared with F6 and F9. Therefore, F2 that was prepared with a CXB:PLGA ratio of 5:100 and showed similar values in terms of particle size (≈273), PDI (0.2) and EE (93.21 %) than F6 and F9 nanoparticles was also included in the following experiment. The characteristics of selected nanoparticles are summarized in Table 7.

All these selected nanoparticles (F2, F6 and F9) showed a negative zeta potential of around −25 mV that could be attributed to the free carboxylic group of PLGA. No statistically significant differences were appreciated between all formulations. These values agree with those obtained by other authors when developed PLGA nanoparticles loaded with other drugs [46,47]. However, it was lower compared to CXB-loaded PLGA nanoparticles developed by Emami and collaborators that showed a zeta potential around −7.5 mV [42].

As displayed in Fig. 6, CXB-loaded nanoparticles showed a relatively spherical shape and a smooth surface. No differences were detected in

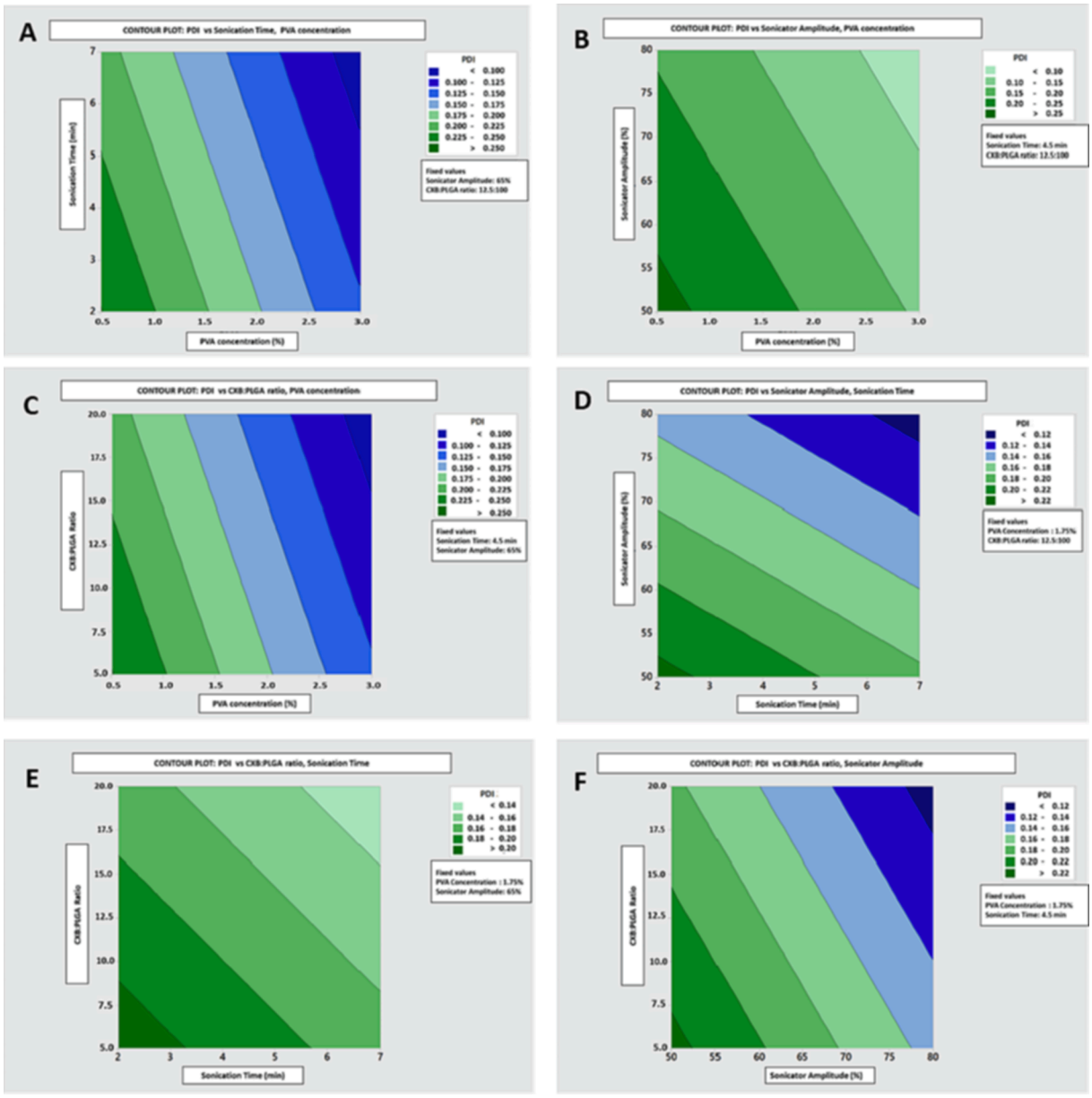

Fig. 3. Contour plots showing the effect of PVA concentration, sonication time, sonicator amplitude and CXB:PLGA ratio on PDI.

Table 5
Statistical ANOVA analysis results of DL and EE (%). * Statistically significant differences (p-value ⟨005).

	Drug loading		EE (%)	
	F-Value	P-value	F-Value	P-value
Regression model	43.09	0.000*	0.24	0.909
Independent Variables				
• PVA concentration (%)	0.09	0.774	0.83	0.392
• Sonication time (min)	0.04	0.849	0.01	0.922
• Amplitude of the sonicator (%)	0.64	0.449	0.05	0.826
• CXB:PLGA ratio	171.59	0.000*	0.05	0.513
ANOVA Lack of fit test				
Lack of fit	0.58	0.762	1.82	0.513

the morphology of the different formulations.

All selected formulations exhibited a controlled drug release (Fig. 7A). F6 and F9 nanoparticles showed a slightly higher burst effect (around 28 % of CXB was released during the first hour) than the F2 formulation, which released around 21 % of celecoxib by this time (Fig. 7B). This higher initial drug release can be attributed to the higher content of CXB, 4 times higher in F6 and F9 formulations, as part of the drug can be exposed on the superficial part of nanoparticles.

F2 formulation showed a tri-phasic release profile with a 1st fast release phase (burst effect) up to 8 h with around 58 % of CXB released, followed by a slower 2nd phase up to day 7. Around 87 % of CXB was released during this period. Finally, a 3rd release phase can be observed from day 7 to day 28, in which CXB is released slowly. Just around 5 % of the drug is released in this period. While the 2nd phase can be fitted to a first-order kinetic ($K = 0.0192$, $R^2 = 0.966$), the 3rd phase fits a zero-order ($K = 0.011$, $R^2 = 0.993$). However, in formulations F6 and F9, a biphasic release profile was observed with a 1st phase of burst release up to 8 h followed by a 2nd slower phase up to day 28 that can be fitted to a zero-order kinetic (F6: $K = 0.084$ $R^2 = 0.974$; F9: $K = 0.113$ $R^2 = 0.932$).

It should be mentioned that the drug release obtained in this work (for at least 10 days in F2 and 28 days in F6 and F9 nanoparticles) is significantly longer compared to CXB-loaded PLGA polymeric nanoparticles obtained by the other authors, that exhibited a controlled drug

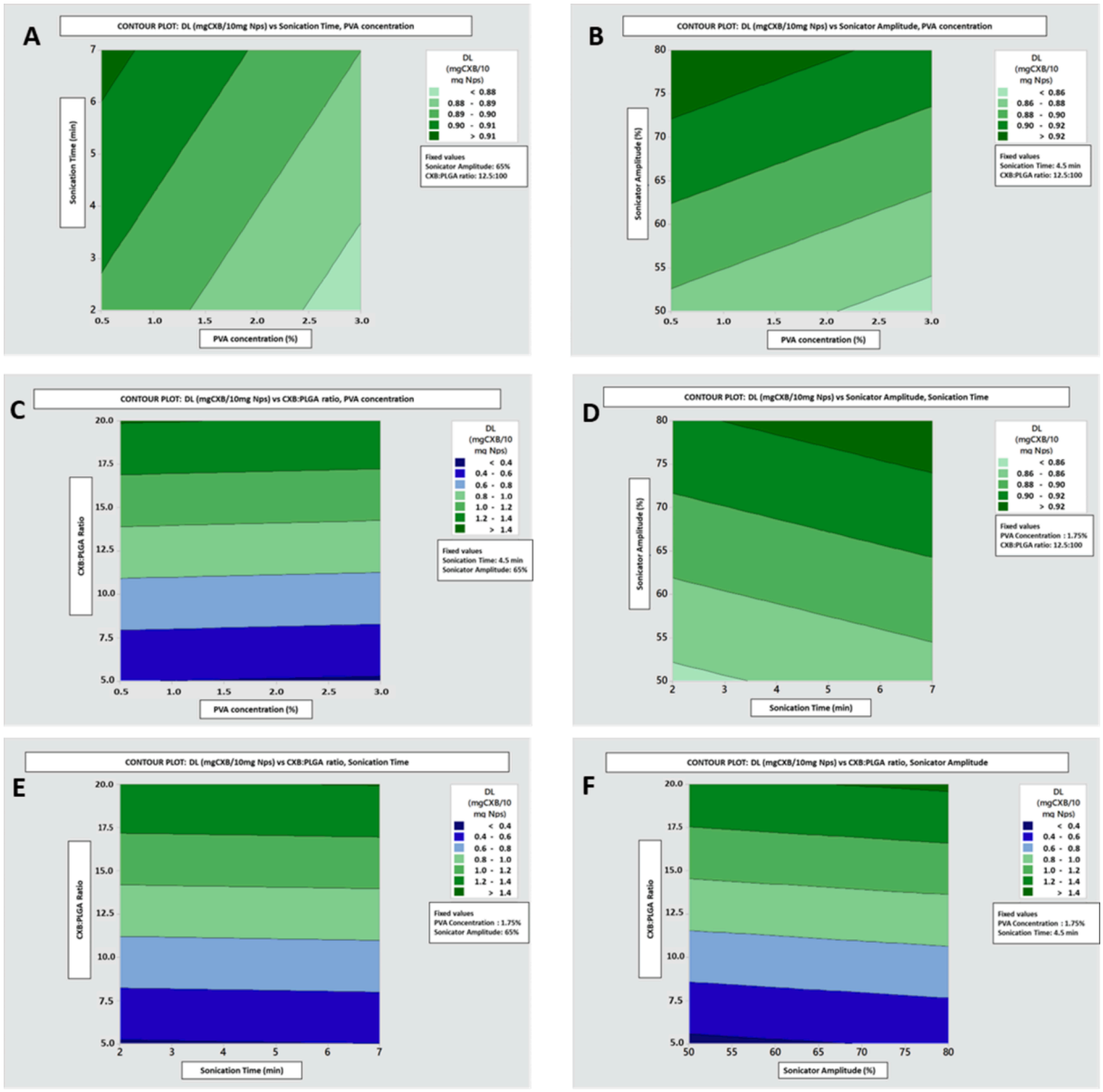

Fig. 4. Contour plots showing the effect of PVA concentration, sonication time, sonicator amplitude and CXB:PLGA ratio on drug loading (DL).

release for around 1–2 days [42,43] although these formulations showed a lower drug content. Considering that the pathological conditions in which this drug is beneficial (cancer and arthritic disorders) are chronic diseases a controlled drug release for>2 days is interesting as would allow a prolonged effect after a single administration.

3.3. Stability studies

CXB-loaded nanoparticles were stable when stored at 5 °C for at least 3 months. In terms of physical stability, similar sizes (around 300 nm) (Fig. 7) and PDI values of 0.18 ± 0.03, 0.16 ± 0.01 and 0.11 ± 0.03 were appreciated in F2, F6 and F9 nanoparticles respectively. No significant changes in zeta potential were observed either showing zeta potential values of −25.73 ± 1.07 mV, −24.89 ± 0.96 mV and −24.09 ± 1.36 mV in F2, F6 and F9 nanoparticles respectively. The superficial charge of nanoparticles is an important factor that affects their stability [48].

In terms of chemical stability, a CXB degradation was not detected in any formulation. After 3 months of storage a drug loading of 0.51 ± 0.89, 1.39 ± 0.17 and 1.50 ± 0.62 mg CXB/ 10 mg Nps were obtained in F2, F6 and F9 nanoparticles respectively which are similar to the initial drug loadings (F2: 0.44 ± 0.48, F6: 1.47 ± 0.46 F9: 1.56 ± 0.12 mg CXB/ 10 mg Nps).

F6 and F9 formulations showed similar characteristics in terms of particle size (≈285 nm), drug loading (≈1.5 mg CXB/10 mg Nps), EE (≈ 90 %) and release profile. They differ in the PVA concentration (3 % vs 0.5 %) and sonicator amplitude (50 % vs 80 %) used during their elaboration. Many authors have demonstrated that an increase in PVA concentration and sonicator amplitude during elaboration protocol causes a faster burst effect [49] as this might facilitates the migration of the drug to the superficial part of nanoparticles during its formation. However, in this study, both formulations showed a similar burst effect and a similar release profile. Due to the similarity of both F6 and F9 formulations, the angiogenesis study was carried out only with the F9 formulation due to its slightly higher CXB content and with F2, due to its different characteristics in terms of drug loading and release profile.

3.4. Angiogenesis studies

As aforementioned, angiogenesis plays a critical role in many

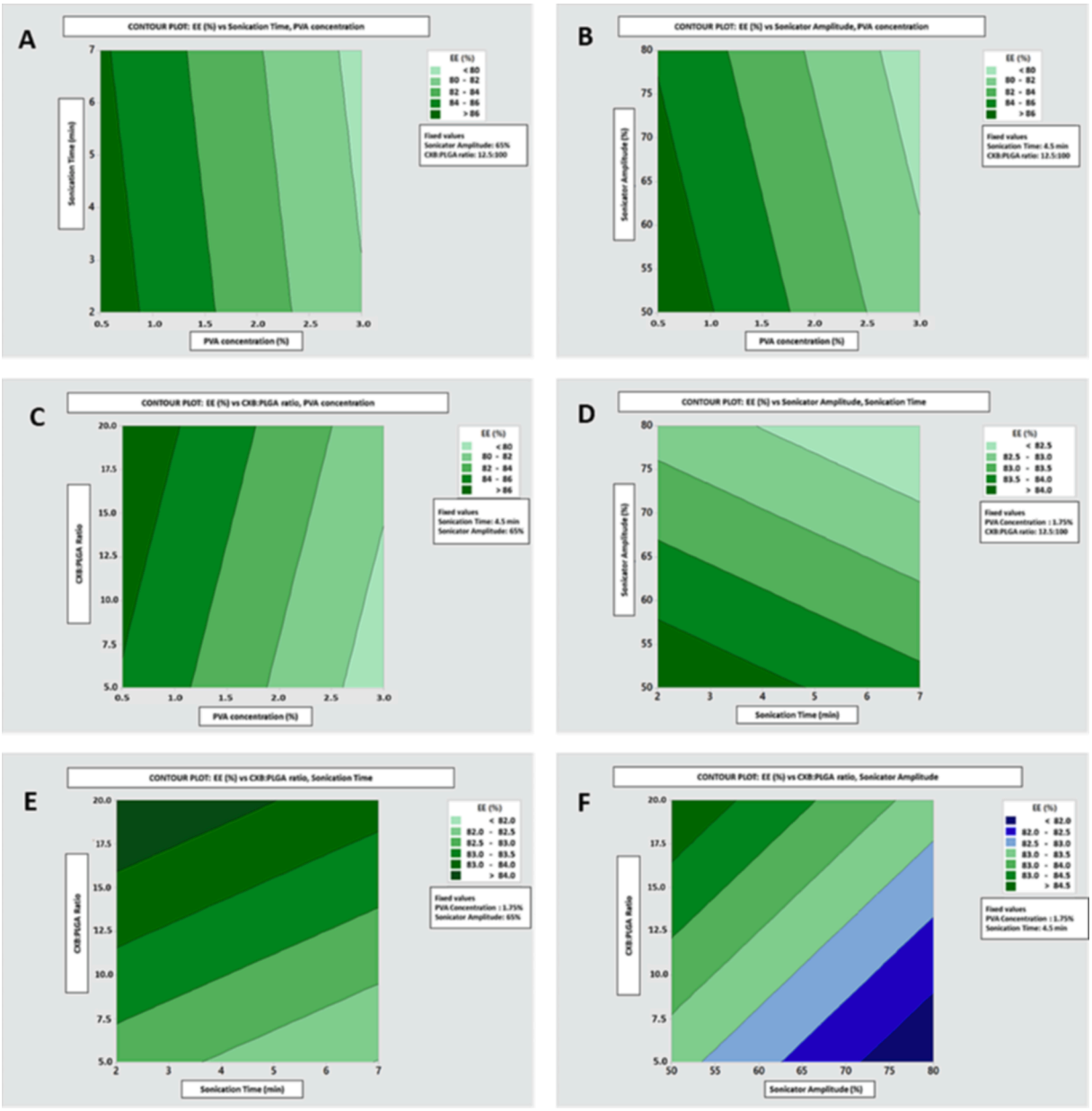

Fig. 5. Contour plots showing the effect of PVA concentration, sonication time, sonicator amplitude and CXB:PLGA ratio on entrapment efficiency (EE).

Table 6
Predicted and observed experimental values of the center checkpoints formulations.

Response	Predicted value	Observed values (average ± sd)	Bias (%)
Particle size (nm)	287.68	284.63 ± 12.75	1.05
PDI	0.169	0.167 ± 0.002	0.79
DL (mg CBX/10 mg Nps)	0.894	0.888 ± 0.02	0.72

pathological conditions such as cancer and arthritic disorders among others [3,4,50]. In this sense, the use of CXB that inhibits angiogenesis would be beneficial [51] and palliate the advance of these diseases. In this work, the antiangiogenic effect of CXB-loaded nanoparticles (F2 and F6) was investigated using the YSM assay, one of the most suitable models for angiogenesis studies [28]. As far as we know the anti-angiogenic effect of CXB-loaded PLGA nanoparticles has not been investigated previously.

As depicted in Fig. 8B both CXB and CXB-loaded nanoparticles exerted an antiangiogenic effect. A significantly ($p < 0.05$) lower amount of all primary, secondary, tertiary and quaternary blood vessels

Table 7
Characteristics of selected CXB-loaded PLGA Nps.

	Process Yield (%)	Particle size (nm)	PDI	Zeta potential	DL (mgCXB/10 mg Nps)	EE(%)	CXB released at 60 min (%)
F2	58.3 ± 6.27	273.03 ± 19.09	0.20 ± 0.01	−25.28 ± 0.94	0.44 ± 0.48	93.21 ± 20.15	20.53 ± 1.96
F6	61.9 ± 2.19	284.66 ± 7.98	0.14 ± 0.04	−23.88 ± 1.24	1.47 ± 0.46	88.63 ± 19.52	34.36 ± 2.86
F9	54.6 ± 10.71	287.80 ± 10.85	0.09 ± 0.02	−24.92 ± 0.92	1.56 ± 0.12	93.85 ± 5.11	37.62 ± 2.39

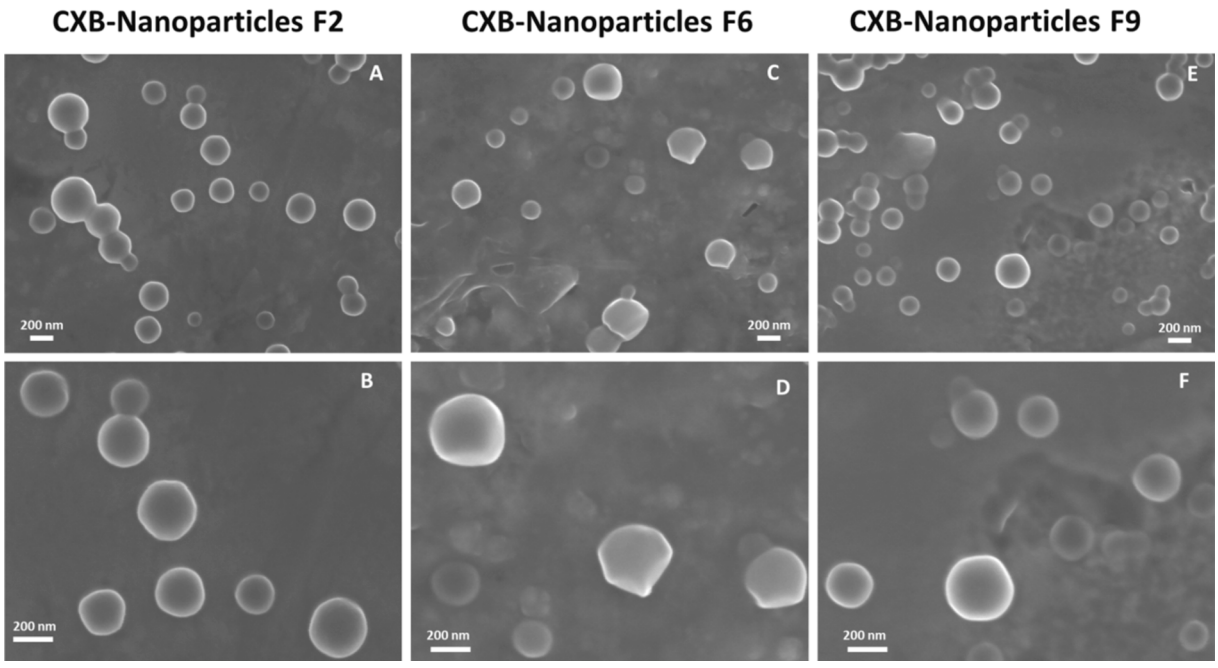

Fig. 6. SEM images of CXB-loaded nanoparticles: F2 (A-B), F6 (C-D) y F9 (E-F).

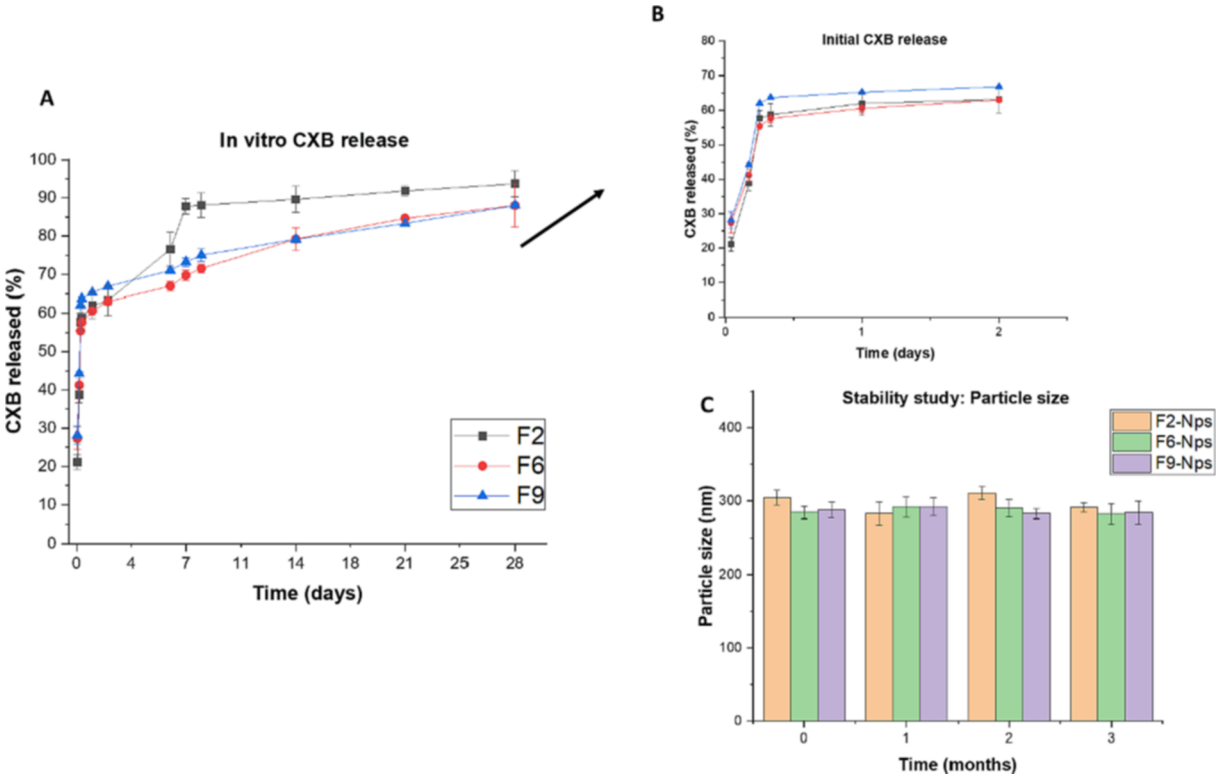

Fig. 7. Complete drug release profile of selected CXB-loaded nanoparticles (A) and during the first 2 days (B) and stability data of particle size expressed as volume diameter (C).

was appreciated in eggs treated with CXB formulations compared to the control (eggs treated with NaCl 0.9 %). Eggs treated with arginine showed a higher number of tertiary and secondary blood vessels as it exerts a pro-angiogenic effect [30].

A reduction in the number of blood vessels above 50 % was achieved with CXB treatments (Fig. 8B), being more pronounced (>65 %) in the case of quaternary blood vessels. Interestingly, a slightly higher antiangiogenic effect was appreciated with CXB-loaded nanoparticles (F2 and F9) compared to CXB in solution. Nevertheless, statistically significant differences (p value < 0.05) were only found in secondary blood vessels with F2 and F9 nanoparticles, and in tertiary blood vessels with F9 nanoparticles. Unloaded nanoparticles did not have an effect on vascularization (data not shown). This could indicate that a constant CXB release, as provided by these nanoparticles, could be beneficial for

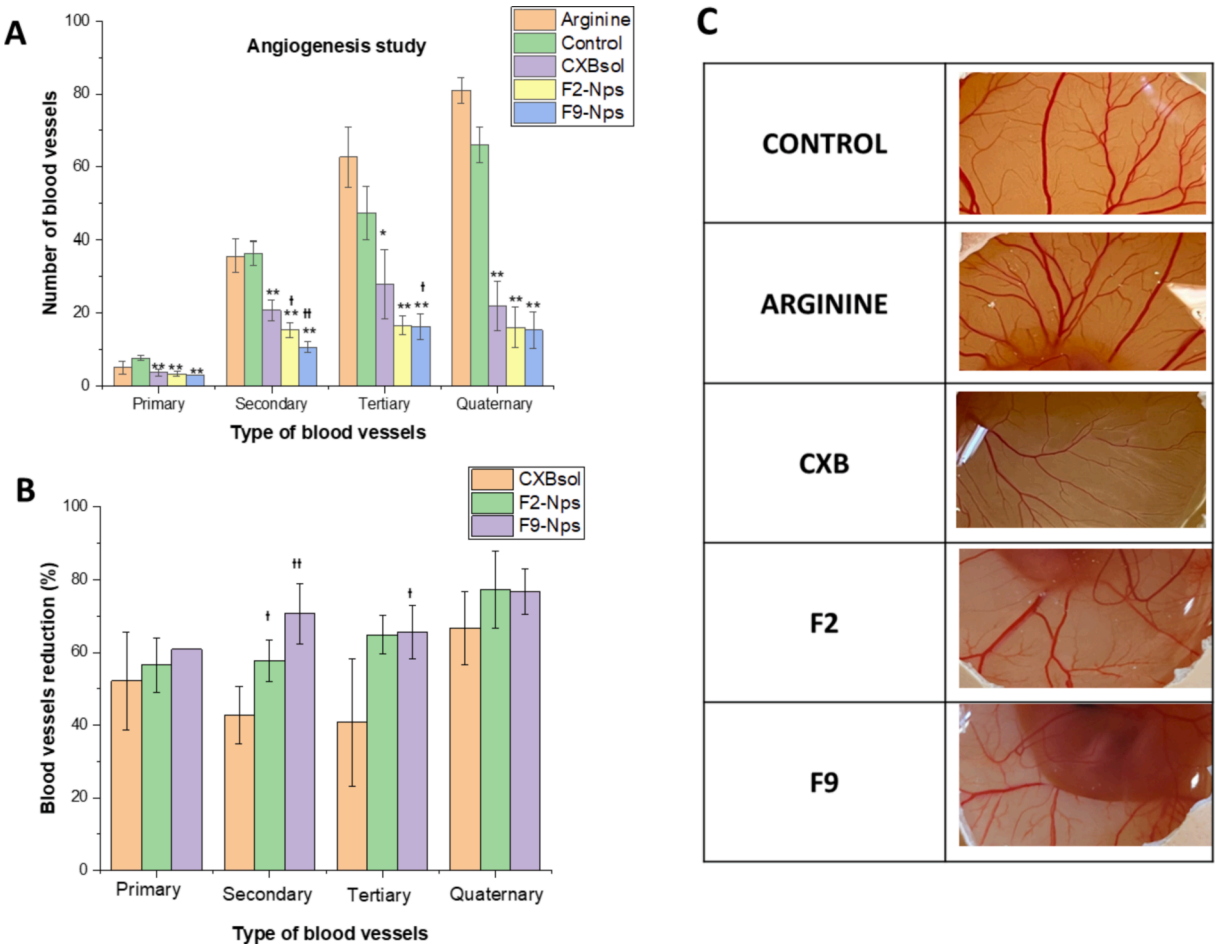

Fig. 8. Angiogenesis study developed in YSM assay: graphs showing the number of blood vessels detected with each treatment (A) and the inhibition percentage observed with CXB formulations (B) and images of treated eggs (C). * and ** indicate statistical significant differences (p-value < 0.05 and 0.01 respectively) with control. † and †† indicate statistically significant differences (p-value < 0.05 and 0.01 respectively) between CXB in solution and CXB-loaded nanoparticles.

its antiangiogenic effect. A similar anti-angiogenic effect was appreciated with both CXB-loaded nanoparticles: F2 and F9.

Other authors have also found that nanoencapsulation increases the anti-angiogenic effects of actives. For example, Dias and collaborators demonstrated that polymeric nanoparticles loaded with imiquimod showed a superior antiangiogenic effect than free imiquimod in CAM assay [20]. Similar results were reported by Carvalho et. al who showed the superior antiangiogenic effect of curcumin-loaded polymeric nanoparticles [21].

It has been mentioned that F9 has been selected as the most suitable CXB-loaded nanoparticle formulation due to its higher drug loading (1.56 mg CXB/10 mg Nps).

4. Conclusions

The Plackett-Burman design performed in this study revealed that PVA concentration (0.5–3 %) was the most influential factor on the particle size and polydispersion index of celecoxib-loaded PLGA nanoparticles prepared by the solvent extraction evaporation method. The higher the PVA concentration, the smaller the particle size and the lower the polydispersity. Sonication time (2–7 min) and sonicator amplitude (50–80 %) also had a negative statistically significant influence on particle size. However, of these two variables, only the change in sonicator amplitude had a significant effect on the polydispersity index. It should be noted that neither of these variables influenced on the loading and encapsulation efficiency. F9 nanoparticles that were prepared using PVA at 0.5 %, a sonication time of 7 min, a sonicator amplitude of 80 % and a CXB:PLGA ratio of 20:100 were selected as the most suitable CXB-formulation. These nanoparticles showed a suitable particle size (≈290 nm) for parenteral administration, low polydispersion (PDI < 0.1), a high drug loading (1.56 mg CXB/10 mg Nps) and a controlled drug release for 28 days. This formulation was stable when stored at 4 °C and demonstrated a better antiangiogenic effect than free CXB in the YSM assay. Consequently, these nanoparticles represent a promising nanocarrier to administer CXB and optimize its therapeutic use in the disorders with pathological angiogenesis such as cancer and arthritic diseases.

Declaration of Competing Interest

The authors declare that they have no known competing financial interests or personal relationships that could have appeared to influence the work reported in this paper.

Data availability

The authors are unable or have chosen not to specify which data has been used.

Acknowledgements

This work was supported by the Santander-UCM research group “Formulation and bioavailability of new drug products” (Ref. UCM-910939) (Complutense University of Madrid, Spain). Irene Lozza has

been awarded a “Perfezionamento all’estero” (Ref:398 of 19 89 – area Cun 05) Biological science grant from the University of “La Sapienza” of Rome.

References

[1] L. Chen, et al., The role of CD44 in pathological angiogenesis, Faseb J. 34 (10) (2020) 13125–13139.
[2] Q. Ma, R.J. Reiter, Y. Chen, Role of melatonin in controlling angiogenesis under physiological and pathological conditions, Angiogenesis 23 (2) (2020) 91–104.
[3] R. Lugano, M. Ramachandran, A. Dimberg, Tumor angiogenesis: causes, consequences, challenges and opportunities, Cell Mol. Life Sci. 77 (9) (2020) 1745–1770.
[4] H.A. Elshabrawy, et al., The pathogenic role of angiogenesis in rheumatoid arthritis, Angiogenesis 18 (4) (2015) 433–448.
[5] C.-M. Su, C.-Y. Huang, C.-H. Tang, Characteristics of resistin in rheumatoid arthritis angiogenesis, Biomarkers Med. 10 (6) (2016) 651–660.
[6] Y. Wang, et al., Geniposide downregulates the VEGF/SphK1/S1P pathway and alleviates angiogenesis in rheumatoid arthritis in vivo and in vitro, Phytother. Res. 35 (8) (2021) 4347–4362.
[7] O. de Labry, A. Lima, et al., Safety considerations during prescription of non-steroidal anti-inflammatory drugs (NSAIDs), through a review of systematic reviews, An. Sist. Sanit. Navar. 44 (2) (2021) 261–273.
[8] S. Bindu, S. Mazumder, U. Bandyopadhyay, Non-steroidal anti-inflammatory drugs (NSAIDs) and organ damage: a current perspective, Biochem. Pharmacol. 180 (2020), 114147.
[9] S. Consalvi, et al., Therapeutic potential for coxibs-nitric oxide releasing hybrids in cystic fibrosis, Eur. J. Med. Chem. 210 (2021), 112983.
[10] B. Cohen, C.V. Preuss, *Celecoxib*, in: *StatPearls*, StatPearls Publishing Copyright © 2022, StatPearls Publishing LLC.: Treasure Island (FL), 2022.
[11] A. Qadir, et al., Synergistic effect of bevacizumab and celecoxib on angiogenesis in vitro using human umbilical vein endothelial cells, Int. J. Clin. Pharmacol. Ther. 58 (12) (2020) 696–702.
[12] S. Liang, et al., Celecoxib reduces inflammation and angiogenesis in mice with adenomyosis, Am. J. Transl. Res. 13 (4) (2021) 2858–2866.
[13] N. Papageorgiou, et al., Celecoxib for the treatment of atherosclerosis, Expert Opin. Invest. Drugs 25 (5) (2016) 619–633.
[14] A.A. El-Malah, et al., Selective COX-2 inhibitors: road from success to controversy and the quest for repurposing, Pharmaceuticals (Basel) 15 (7) (2022).
[15] Information., N.C.f.B., “PubChem Compound Summary for CID 2662, Celecoxib” PubChem,https://pubchem.ncbi.nlm.nih.gov/compound/Celecoxib. Accessed 14 April, 2022. 2022.
[16] G.M. Pontes-Quero, et al., Modulation of inflammatory mediators by polymeric nanoparticles loaded with anti-inflammatory drugs, Pharmaceutics 13 (2) (2021).
[17] X. Wen, X. Huang, H. Wu, Development of a novel intraarticular injection of diclofenac for the treatment of arthritis: a preclinical study in the rabbit model, Acta Biochim. Pol. 68 (1) (2021) 71–76.
[18] R.I. El-Gogary, M.A. Khattab, H. Abd-Allah, Intra-articular multifunctional celecoxib loaded hyaluronan nanocapsules for the suppression of inflammation in an osteoarthritic rat model, Int. J. Pharm. 583 (2020), 119378.
[19] J.R. Madan, et al., Formulation and in vitro evaluation of casein nanoparticles as carrier for celecoxib, Adv. Pharm. Bull. 10 (3) (2020) 408–417.
[20] M.F. Dias, et al., In vivo evaluation of antitumoral and antiangiogenic effect of imiquimod-loaded polymeric nanoparticles, Biomed. Pharmacother. 103 (2018) 1107–1114.
[21] F.B. de Carvalho, et al., Evaluation of curcumin-loaded polymeric nanocapsules with different coatings in chick embryo model: influence on angiogenesis, teratogenesis and oxidative stress, Pharmacol. Rep. 73 (2) (2021) 563–573.
[22] A.I. Fraguas-Sánchez, et al., CBD loaded microparticles as a potential formulation to improve paclitaxel and doxorubicin-based chemotherapy in breast cancer, Int. J. Pharm. 574 (2020), 118916.
[23] T. Rawal, S. Patel, S. Butani, Chitosan nanoparticles as a promising approach for pulmonary delivery of bedaquiline, Eur. J. Pharm. Sci. 124 (2018) 273–287.
[24] E. Barcia, et al., Nanotechnology-based drug delivery of ropinirole for Parkinson’s disease, Drug Delivery 24 (1) (2017) 1112–1123.
[25] M. Vera, et al., New celecoxib multiparticulate systems to improve glioblastoma treatment, Int. J. Pharm. 473 (1–2) (2014) 518–527.
[26] A.I. Fraguas-Sánchez, et al., PLGA nanoparticles for the intraperitoneal administration of CBD in the treatment of ovarian cancer: in vitro and in Ovo assessment, Pharmaceutics 12 (5) (2020).
[27] E. Pape, et al., Rapamycin-loaded Poly(lactic-co-glycolic) acid nanoparticles: Preparation, characterization, and in vitro toxicity study for potential intra-articular injection, Int. J. Pharm. 609 (2021), 121198.
[28] A.I. Fraguas-Sánchez, C. Martín-Sabroso, A.I. Torres-Suárez, The chick embryo chorioallantoic membrane model: a research approach for ex vivo and in vivo experiments, Curr. Med. Chem. (2021).
[29] D. Ribatti, T. Annese, R. Tamma, The use of the chick embryo CAM assay in the study of angiogenic activiy of biomaterials, Microvasc. Res. 131 (2020), 104026.
[30] M.N. As, et al., Establishment of an in ovo chick embryo yolk sac membrane (YSM) assay for pilot screening of potential angiogenic and anti-angiogenic agents, Cell Biol. Int. 42 (11) (2018) 1474–1483.
[31] C. Maes, et al., Use of new glycerol-based dendrimers for essential oils encapsulation: optimization of stirring time and rate using a Plackett-Burman design and a surface response methodology, Foods 10 (2) (2021).
[32] S.R. Shah, et al., Application of Plackett-Burman screening design for preparing glibenclamide nanoparticles for dissolution enhancement, Powder Technol. 235 (2013) 405–411.
[33] H. Vardhan, et al., Long-circulating polyhydroxybutyrate-co-hydroxyvalerate nanoparticles for tumor targeted docetaxel delivery: formulation, optimization and in vitro characterization, Eur. J. Pharm. Sci. 99 (2017) 85–94.
[34] K.Y. Hernández-Giottonini, et al., PLGA nanoparticle preparations by emulsification and nanoprecipitation techniques: effects of formulation parameters, RSC Adv. 10 (8) (2020) 4218–4231.
[35] P. Rafiei, A. Haddadi, A robust systematic design: optimization and preparation of polymeric nanoparticles of PLGA for docetaxel intravenous delivery, Mater. Sci. Eng., C 104 (2019), 109950.
[36] F. Madani, et al., Investigation of effective parameters on size of paclitaxel loaded PLGA nanoparticles, Adv. Pharm. Bull. 8 (1) (2018) 77–84.
[37] K.B. Almeida, et al., PLGA nanoparticles optimized by Box-Behnken for efficient encapsulation of therapeutic Cymbopogon citratus essential oil, Colloids Surf. B Biointerfaces 181 (2019) 935–942.
[38] M. Elmowafy, et al., Long-acting paliperidone parenteral formulations based on polycaprolactone nanoparticles; the influence of stabilizer and chitosan on in vitro release, protein adsorption, and cytotoxicity, Pharmaceutics 12 (2) (2020) 160.
[39] H. Thakkar, R. Kumar Sharma, R.S. Murthy, Enhanced retention of celecoxib-loaded solid lipid nanoparticles after intra-articular administration, Drugs R D 8 (5) (2007) 275–285.
[40] M. Danaei, et al., Impact of particle size and polydispersity index on the clinical applications of lipidic nanocarrier systems, Pharmaceutics 10 (2) (2018).
[41] Y. Lee, E. Sah, H. Sah, Chemical approach to solvent removal during nanoencapsulation: its application to preparation of PLGA nanoparticles with non-halogenated solvent, J. Nanopart. Res. 17 (11) (2015) 453.
[42] J. Emami, et al., Formulation and optimization of celecoxib-loaded PLGA nanoparticles by the Taguchi design and their in vitro cytotoxicity for lung cancer therapy, Pharm. Dev. Technol. 20 (7) (2015) 791–800.
[43] T.H. Kim, et al., Preparation of polylactide-co-glycolide nanoparticles incorporating celecoxib and their antitumor activity against brain tumor cells, Int J Nanomedicine 6 (2011) 2621–2631.
[44] B. Crivelli, et al., Silk fibroin nanoparticles for celecoxib and curcumin delivery: ROS-scavenging and anti-inflammatory activities in an in vitro model of osteoarthritis, Eur. J. Pharm. Biopharm. 137 (2019) 37–45.
[45] R. Ismail, et al., Synthesis and statistical optimization of poly (lactic-co-glycolic acid) nanoparticles encapsulating GLP1 analog designed for oral delivery, Pharm. Res. 36 (7) (2019) 99.
[46] P. Marcianes, et al., Surface-modified gatifloxacin nanoparticles with potential for treating central nervous system tuberculosis, Int. J. Nanomed. 12 (2017) 1959–1968.
[47] H. Yang, et al., Design of poly(lactic-co-glycolic acid) (PLGA) nanoparticles for vaginal co-delivery of griffithsin and dapivirine and their synergistic effect for HIV prophylaxis, Pharmaceutics 11 (4) (2019).
[48] E.B. Manaia, et al., Physicochemical characterization of drug nanocarriers, Int. J. Nanomed. 12 (2017) 4991–5011.
[49] I. Takeuchi, Y. Kato, K. Makino, Effects of polyvinyl alcohol on drug release from nanocomposite particles using poly (L-lactide-co-glycolide), J. Oleo Sci. 70 (3) (2021) 341–348.
[50] X. Hu, et al., RGS1 silencing inhibits the inflammatory response and angiogenesis in rheumatoid arthritis rats through the inactivation of Toll-like receptor signaling pathway, J. Cell. Physiol. 234 (11) (2019) 20432–20442.
[51] R.M. El-Sayed, Y.M. Moustafa, M.F. El-Azab, Evening primrose oil and celecoxib inhibited pathological angiogenesis, inflammation, and oxidative stress in adjuvant-induced arthritis: novel role of angiopoietin-1, Inflammopharmacology 22 (5) (2014) 305–317.